Research Article | Vol. 29, No. 11 / 24 May 2021 / Optics Express 17286
Optics EXPRESS

Ultimate conversion efficiency of second harmonic generation in all-dielectric resonators of quasi-BICs in consideration of nonlinear refraction of dielectrics

TINGYIN NING,[1,2] XIN LI,[1,2] ZHONGSHUAI ZHANG,[1,2] YANYAN HUO,[1,2] QINGYANG YUE,[1,2] LINA ZHAO,[1,2] AND YUANMEI GAO[1,2,*]

[1]*Shandong Provincial Engineering and Technical Center of Light Manipulations & Shandong Provincial Key Laboratory of Optics and Photonic Device, School of Physics and Electronics, Shandong Normal University, Jinan 250358, China*
[2]*Collaborative Innovation Center of Light Manipulations and Applications, Shandong Normal University, Jinan 250358, China*
[*]*gaoyuanmei@sdnu.edu.cn*

Abstract: We investigate second harmonic generation (SHG) in all-dielectric resonance nanostructures of high-Q factors assisted by quasi-bound states in the continuum (quasi-BICs). The typical resonators, e.g., guided-mode resonance gratings and asymmetric metasurfaces, fabricated by AlGaAs were numerically studied with the consideration of nonlinear refraction of AlGaAs. The resonance peak and line-shape of linear transmission and SHG spectra in the resonators can be dramatically changed under intense pump intensities. The SHG conversion efficiency in the nanostructures working at quasi-BICs is much lower than the traditionally expected values without considering the nonlinear refraction of dielectrics. The ultimate SHG conversion efficiency is finally obtained. The investigation has the significance for the design and understanding of efficient nonlinear metasurfaces of high-Q factors.

1. Introduction

Nonlinear metasurfaces have attracted more attention and growing interests in the nanophotonics community due to their diverse functionalities, such as, high-integrated on-chip frequency conversion [1,2], light shaping at new frequencies [3,4], nonlinear imaging and holography [5–7], nonlinear optical bistability [8], etc. Different from the bulk nonlinear materials, in which the phase matching condition must be considered for the frequency conversion processes, such as second harmonic generation (SHG) and third harmonic generation (THG), to achieve the maximum output of nonlinear signals, metasurface of the dimension along the light propagation is in the subwavelength domain and the phase matching is almost free. To achieve the efficient conversion efficiency of nonlinear process in metasurfaces, the resonance mode is essentially required to confine the light in the ultra-small volume to enhance the local field. For example, the metasurfaces fabricated by noble metals of significantly enhanced local field at the localized surface plasmon resonance frequency have been widely studied [1]. However, the conversion efficiency of nonlinear optical processes in plasmonic metasurfaces is relatively small. The conversion efficiency of SHG and THG in typical plasmonic metasurface based on split-ring resonators is in the order of 10^{-11} and 10^{-12}, respectively [9,10]. Even in the mode matching plasmonic nanoantennas, the maximum SHG conversion efficiency is limited up to 6.4×10^{-9} [11]. Such low conversion efficiency can be ascribed to the intrinsic loss and low damage threshold of pump light in metallic nanostructures.

All-dielectric resonant nonlinear metasurfaces have drawn more interesting and been intensively studied due to the large nonlinear susceptibility, low and even zero loss, and high damage threshold

#427355 https://doi.org/10.1364/OE.427355
Journal © 2021 Received 8 Apr 2021; revised 13 May 2021; accepted 14 May 2021; published 19 May 2021

Optics EXPRESS

of pump light in dielectrics [12–14]. Particularly, optical bound states in the continuum (BICs), as the recently emerged concept which can achieve ultra-high Q factor and field enhancement factor [15], have been employed for low threshold lasing [16,17], biosensing [18,19], switching [20], etc. Efficient harmonic generation in the nanostructures of quasi-BICs was widely reported recently. Liu *et al*, experimental obtained the THG conversion efficiency in asymmetric silicon metasurface of high-Q factor in quasi-BIC around 1×10^{-6} at peak intensity 0.1 GW/cm^2 [21]. Carletti *et al*, numerically reports the BIC-driven intrinsic SHG conversion efficiency in the AlGaAs cylinder achieves the value as high as 2×10^{-2} W^{-1} [22]. Kang *et al*, numerically reported that SHG conversion efficiency in asymmetric $LiNbO_3$ metasurfaces of quasi-BICs arrives 0.49% under the peak pump intensity of 3.3 kW/cm^2 [23]. Han *et al*, numerically reported the significantly enhanced SHG in AlGaAs antenna arrays working in the quasi-BICs of efficiency around 10% at the pump intensity of 5 MW/cm^2 [24]. Rocco *et al*, alternatively investigated SHG from AlGaAs nanoantennas with epsilon-near-zero (ENZ) materials as the substrates, and the boosted SHG conversation efficiency on the order of 10^{-3} for a pump intensity of 1.6 GW/cm^2 was obtained [25]. The vertical SHG with engineered radiation patterns in asymmetric AlGaAs nanoantennas of SHG conversion efficiency 1.6×10^{-5} at pump intensity of 1.6 GW/cm^2 was reported by the same group [26]. However, in these numerical works, the intrinsic third-order optical nonlinearity in the dielectric, i.e. nonlinear refraction and absorption, was neglected. Due to the ultra-high Q factor and dramatically enhanced local field in the cavity, the refractive index and extinction coefficient of dielectric will be changed even when the intensity of pump light is relatively low, and thus affect the resonance spectra of ultra-narrow linewidth under the quasi-BICs. The optical harmonic generation in the dielectric will then be significantly affected along with the change of linear optical spectra.

In this work, we investigate the conversion efficiency of harmonic generation in all-dielectric resonance nanostructures working at quasi-BICs considering the intrinsic third-order optical nonlinearity in dielectrics. We mainly focus our study on the SHG in guided-mode resonance grating (GMR) nanostructures and asymmetric metasurfaces fabricated by $Al_{0.18}Ga_{0.82}As$ (AlGaAs) with high-Q resonances governed by quasi-BICs. The nonlinear refraction n_2 of AlGaAs and the negligible two- and three-photon absorption in our concerned resonance wavelengths are fully considered to obtained the ultimate SHG conversion efficiency in these resonance nanostructures of quasi-BICs.

2. Numerical models and method

Two typical nanostructures, namely GMR and asymmetric metasurface, based on AlGaAs fabricated on the semi-infinite fused silica with high-Q resonances working at quasi-BICs are studied. The schematic GMR structure is composed of a four-part grating layer and a waveguide layer, as shown in Fig. 1(a). The typical structure was also depicted in the Refs. [27,28]. The first and third parts of grating are made of dielectrics AlGaAs of width d_a, and the second and fourth parts are filled with air of width d_b and d_c, respectively. So, the periodic of grating layer Λ is $\Lambda = 2*d_a+d_b+d_c$. Here the value of d_a is set as 0.2Λ, then $d_b=d-\Delta d$ and $d_c=d+\Delta d$ with $d=0.3\Lambda$. An adjustable geometric parameter δ is defined as $\delta=\Delta d/d \in [0,1]$ to note the difference of d_b and d_c. The thickness of grating layer and waveguide layer (AlGaAs) is denoted as d_g and d_w, respectively. The light of transverse magnetic (TM) polarization ($\boldsymbol{H}$ along z-axis) and angle of incidence $\phi = 5°$ is considered. In addition, the schematic unit cell of an asymmetric metasurface consisting of a square lattice of tilted AlGaAs-bar pairs is shown in Fig. 3(a). The asymmetry parameter in such structure is the angle θ between the long axis of the bar and the y-axis. The light of polarization along x-axis shines on the structure at normal incidence.

Optics EXPRESS

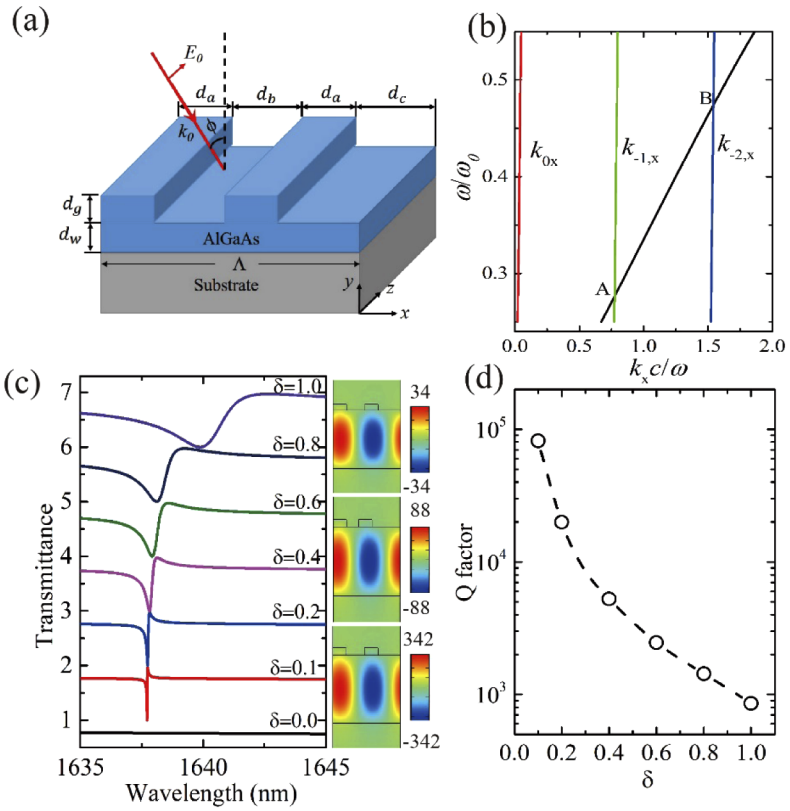

Fig. 1. (a) Schematic of a unit cell of GMR structure. Waveguide layer and grating part are fabricated by AlGaAs, and fused silica is used as a substrate. Geometrical parameters: Λ=600 nm, d_g = 50 nm, d_w=450 nm, d_a=0.2Λ, d_b=d-Δd, d_c=d+Δd with d=0.3Λ and Δd=δ*d with δ∈[0,1]. The incidence light of TM-polarization and angle of incidence ϕ. (b) Dispersion relation of the TM_0 guided mode in the waveguide layer (black solid line), and tangential component of the wave vector k_x=$k_{m,x}$ (m=0,−1,−2) under the angle of incidence 5°. (c) The transmission spectra of GMR nanostructures of different δ. The magnetic field |Hz/H_0| distributions at the corresponding resonance modes are shown on the right side. (d) Dependence of Q factor on the parameter δ.

In the framework of the depleted pump condition, the fundamental and SHG fields in the frequency domain can be expressed as [29]

$$\nabla \times \nabla \times \mathbf{E}(\omega) - k_0^2 \mathbf{E}(\omega) = \mu_0 \omega^2 \mathbf{P}(\omega) \tag{1}$$

$$\mathbf{P}(\omega) = \varepsilon_0 \chi^{(1)}(\omega)\mathbf{E}(\omega) + \varepsilon_0 \chi^{(2)}(\omega : 2\omega, -\omega) : \mathbf{E}(2\omega)\mathbf{E}^*(\omega) + \varepsilon_0 \chi^{(3)}(\omega : \omega, \omega, -\omega) : \mathbf{E}(\omega)\mathbf{E}(\omega)\mathbf{E}^*(\omega) \tag{2}$$

$$\nabla \times \nabla \times \mathbf{E}(\Omega) - \varepsilon_2 k_2^2 \mathbf{E}(\Omega) = \mu_0 \Omega^2 \mathbf{P}(\Omega) \tag{3}$$

$$\mathbf{P}(\Omega) = \varepsilon_0 \chi^{(2)}(\Omega) : \mathbf{E}(\omega)\mathbf{E}(\omega) + \varepsilon_0 \chi^{(3)}(\Omega : \Omega, \Omega, -\Omega) : \mathbf{E}(\Omega)\mathbf{E}(\Omega)\mathbf{E}^*(\Omega) \tag{4}$$

where ω and Ω=2ω are the angular frequency of fundamental and SHG field, $\mathbf{E}(\omega)$ and $\mathbf{E}(\Omega)$ are fundamental and SHG electric field, $\mathbf{P}(\omega)$ and $\mathbf{P}(\Omega)$ are liner and SH polarization, respectively. k_0=ω/c, and k_2=Ω/c are the wave vectors of fundamental and SHG beam, respectively, where

Optics EXPRESS

c is the speed of light in a vacuum. μ_0 and ε_0 are the vacuum permeability and permittivity, respectively. ε_2 is the relative permittivity of materials at SH frequency. $\chi^{(1)}(\omega)$ is the linear susceptibility of AlGaAs at the fundamental frequency, and the relative permittivity of AlGaAs $\varepsilon_1=1+\chi^{(1)}(\omega)=n^2$, where n is the linear refractive index of AlGaAs that is taken from the Ref. [30]. $\chi^{(3)}(\omega:\omega,\omega,-\omega)$ and $\chi^{(3)}(\Omega:\Omega,\Omega,-\Omega)$ are the third-order nonlinear susceptibility of AlGaAs at fundamental and SH frequency, respectively. The two- and three-photon absorption in AlGaAs at the resonance wavelength concerned in this article is negligible. So the $\chi^{(3)}(\omega:\omega,\omega,-\omega)$ is a pure real number. The polarization at SH frequency induced by Kerr nonlinearity (the second term of Eq. (4)) can be neglected, which is orders of magnitude smaller than the polarization from SHG (the first term of Eq. (4)). $\chi^{(3)}(\omega:\omega,\omega,-\omega)$ of the SI-unit m^2/V^2 equals to $4\varepsilon_0 cn^2 n_2/3$, where n_2 is the coefficient of the intensity-dependent refractive index [31]. The change of the refractive index Δn considering the Kerr nonlinearity of dielectrics can written as $\Delta n = n_2 I$ with the I the local intensity in the dielectric materials. The n_2 in AlGaAs is around 1×10^{-17} m^2/W [32], and then $\chi^{(3)}(\omega:\omega,\omega,-\omega)$ is about 1.1×10^{-18} m^2/V^2 in the range of 1.6 μm to 2 μm. The non-zero tensor components of the second order susceptibility are $\chi^{(2)}_{ijk}$ = 200 pm/V with $i\neq j\neq k$ [33].

The coupled Eqs. (1)–(4) can be numerically solved using finite element method (Comsol Multiphysics, Wave Optics Module) to obtain the linear optical transmission and transmitted SHG from the nanostructures. Particularly, the polarization at fundamental (Eq. (2)) and SH frequency (Eq. (4)) can be directly written into the built-in settings of the module. The details can refer the Ref. [27]. In this work, we use the definition of SHG conversion efficiency $\eta=P_{\mathrm{SHG}}/P_{\mathrm{pump}}$, where P_{pump} and P_{SHG} are the power of fundamental pump light and SHG light, respectively. Considering the damage threshold of AlGsAs is around a few GW/cm^2 [34], we limit the input pump intensity up to 1 MW/cm^2, which corresponds to the several GW/cm^2 inside the AlGsAs nanostructures considering the enhancement factor of electric field at the resonance modes.

3. Results and discussion

We first demonstrate the results obtained from the GMR nanostructures. The propagation constant of the guided mode β in the waveguide layer can be analytically determined [28], as shown in Fig. 1(b). The simple three-layer mode, namely air-waveguide-substrate, is used. In the figure, the ω_0 is defined as $2\pi c/d_{\mathrm{w}}$ with c the speed of light in the vacuum. The tangential component of the wave vector k_{x} in the air background and grating layer is written as $k_{\mathrm{x}}=k_{0\mathrm{x}}=k_0\sin\theta$ and $k_{\mathrm{x}}=k_{\mathrm{m,x}}=k_0\sin\theta$-$mG$ ($m=\pm1, \pm2,\ldots$), respectively, where $G=2\pi/\Lambda$ is the reciprocal lattice in the nanostructure of $\delta\neq0$, and becomes $G'=2\pi/(\Lambda/2)$ for the nanostructure when $\delta=0$. The crossing points between β and k_{x} in the figure mean that the phase matching condition is satisfied, namely, GMR. The crossing point A corresponds to the negative first-order mode in the nanostructure of $\delta\neq0$ of the value $0.276\omega_0$ (1627 nm). When $\delta=0$, the negative first-order mode in such the nanostructure becomes the negative second-order mode in the nanostructure of $\delta\neq0$ considering the relation of the reciprocal lattice G' and G. Thus, the crossing point B corresponds to the negative second-order mode in the nanostructure of $\delta\neq0$ but the negative first-order mode in the nanostructure of $\delta=0$. So the excitable odd-order modes of GMR in the nanostructure of $\delta\neq0$ cannot be excited in the nanostructure of $\delta=0$, but the change of parameter δ from zero to nonzero can excite the odd-order guided modes called quasi-BICs of a high Q factor in GMR nanostructure, as discussed in Refs. [27,28].

The transmission spectra in the nanostructures of different δ is shown in Fig. 1(c). The resonance wavelength is around 1637.72 nm, which is some larger than the theoretical value (1627 nm). It is because that the real refractive index upon the waveguide layer is not 1 of air but the effective index of grating layer and air. The resonance wavelength shifts and becomes broader with the increase of δ due to the change of the distribution of refractive index upon the waveguide layer. The electric field distributions in the nanostructures of different δ=0.1, 0.4

Optics EXPRESS

and 1.0 are shown on the right side of Fig. 1(c), respectively. The waveguide modes are clearly formed and the enhancement factor in the structure of δ=0.1 arrives up to 342. The Q factors are calculated in the nanostructures of different δ, as shown in Fig. 1(d). The Q factor reaches up to 8.2×10^4 at δ=0.1. Next, we will focus on the nanostructure of δ=0.1 of high Q factor to study the nonlinear optical response.

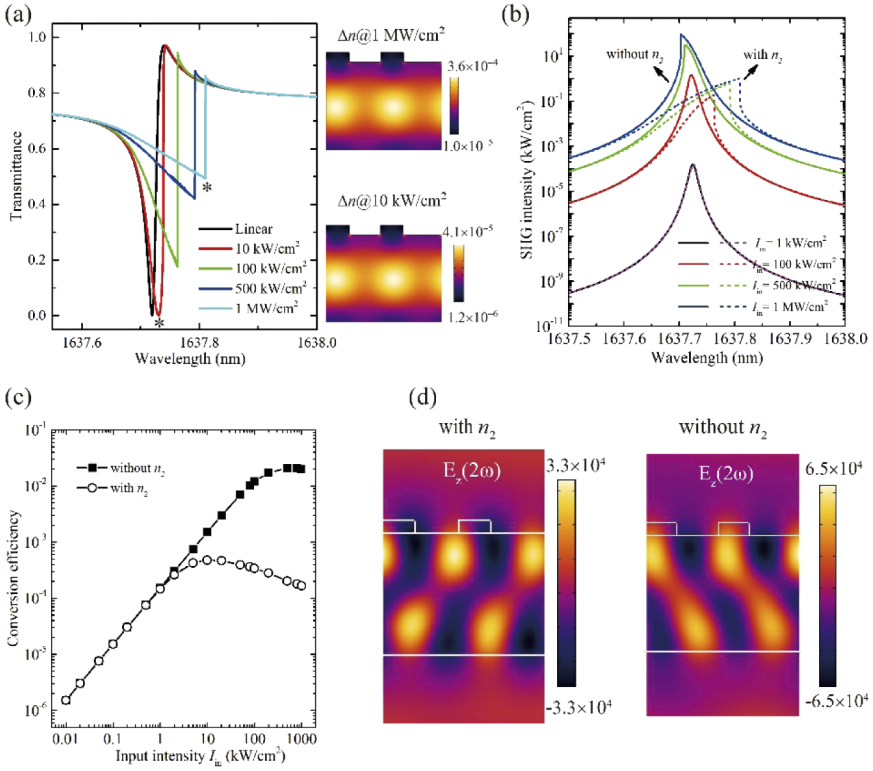

Fig. 2. (a) Linear transmission spectra at different pump intensities and the change of refractive index Δn of AlGaAs layers at pump intensity of 10 kW/cm^2 and 1 MW/cm^2 at the resonance wavelength marked by star is shown, respectively. (b) SHG intensity spectra with and without considering the nonlinear refraction of AlGaAs at different pump intensities. (c) SHG conversion efficiency at the linear resonance wavelength, and (d) electric field distribution of $E_z(2\omega)$ at second harmonic frequency under pump intensity 10 kW/cm^2 with and without considering the n_2 of AlGaAs in the GMR nanostructure of δ=0.1.

The transmission of the GMR nanostructure considering the nonlinear refraction of AlGaAs under the pump light of intense intensities was studied, as shown in Fig. 2(a). The change of refractive index Δn of the AlGaAs at pump intensity of 10 kW/cm^2 and 1 MW/cm^2 at the respective resonance wavelength is shown. The maximum change of Δn happens in the waveguide layer and is around 4.1×10^{-5} and 3.6×10^{-4} at the two typical pump intensities respectively. The resonance wavelengths have a clear red-shift with the increase of input intensity, and the Fano line-shape of the spectra is also distorted due to the change of refractive index of AlGaAs. Such changes of linear response will thus affect the SHG spectra in the nanostructures, as shown in the Fig. 2(b). We compare the SHG spectra in the nanostructure considering the intrinsic n_2 of AlGaAs with those in the nanostructure without considering n_2 of AlGaAs that was usually neglected in reported literatures [23–27]. Under the relatively lower pump intensity, such as 1 kW/cm^2, the SHG spectra are almost overlapped with each other when considering and without

Optics EXPRESS

considering n_2 of AlGaAs due to the almost unchanged refractive index. The peak of SHG intensity just locates at the resonance wavelength of the nanostructure. With the increase of pump intensity, the SHG peak in the nanostructure without considering n_2 of AlGaAs has a blue-shift due to the raising polarization in Eq. (2) involving the increased SHG field, however, the SHG peak has a red-shift when n_2 of AlGaAs is considered due to the red-shifted resonance wavelength (Fig. 2(a)). If we fix the fundamental wavelength at the resonance wavelength obtained from the linear transmission spectra to observe SHG response, the dependence of SHG conversion efficiency on the input pump intensity is shown in Fig. 2(c). The maximum SHG conversion efficiency in the GMR nanostructure is around 4.8×10^{-4} at the pump intensity of 10 kW/cm^2 when the intrinsic n_2 of AlGaAs is considered, which is much lower than the maximum conversion efficiency in the nanostructure of the value 2.1×10^{-2} without considering n_2 of AlGaAs. The maximum conversion efficiency in the nanostructure considering the intrinsic n_2 of AlGaAs under the pump intensity 1 MW/cm^2 happens at the wavelength around 1637.81 nm of the value 1.2×10^{-3}, which is the ultimate SHG conversion efficiency of the AlGaAs GMR nanostructure. The SHG fields E_z (2ω) considering and without considering n_2 of AlGaAs under the same pump intensity 10 kW/cm^2 are shown in Fig. 2(d). The distribution and value of SHG field are dramatically different due to the difference of refractive index of AlGaAs.

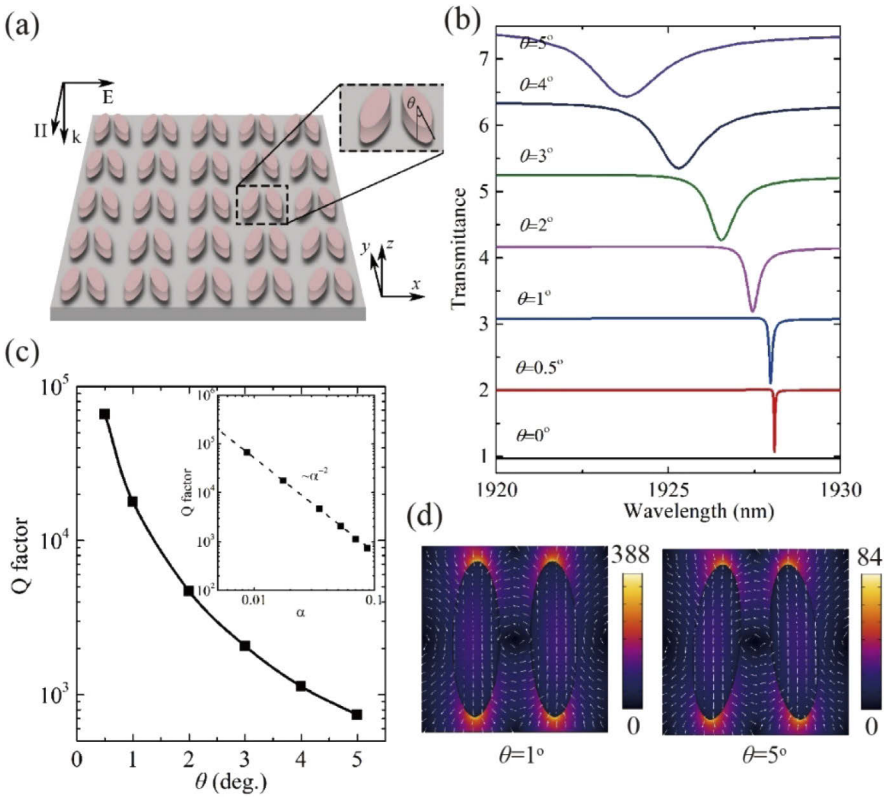

Fig. 3. (a) Schematic of an asymmetric metasurface. Geometrical parameters: square lattice constant 1200 nm, bar semiaxes are 500 and 150 nm, height is 200 nm, and distance between bars (center-to-center) is 500 nm. The rotational angle of the bar is θ. (b) Linear transmission spectra in the metasurfaces of different angle θ. (c) Dependence of the Q factor on the angle θ. Inset shows the linear relation between Q factor and asymmetric parameter α. (d) The electric field $|E/E_0|$ distribution at the resonance wavelength of metasurfaces of angle θ=1° and 5°, respectively.

Optics EXPRESS

We next address the results in the asymmetric metasurfaces consisting of the tilted AlGaAs-bar pairs. The linear transmission spectra in the metasurfaces of different tilted angle θ is shown in Fig. 3(b). The ideal structure of θ=0° supports a symmetry-protected BIC of infinite Q factor. The symmetry-breaking by changing θ leads to the quasi-BIC of high-Q factors. The resonance wavelength at quasi-BIC in the metasurface of angle θ=0.5° is around 1928.08 nm. The transmission spectra shift to blue-side and become broader with the increase of θ. The Q factors in the asymmetry metasurfaces of different θ are shown in Fig. 3(c). The high-Q factor in the metasurface of θ=0.5° reaches up 6.0×10^4. The linear relation of Q factor and the asymmetry parameter α, defined as α=sinθ, is shown in the inset of Fig. 3(c), as reported in the Ref. [35]. The local electric field distributions and polarization states in the asymmetry metasurfaces of θ=1° and 5° at their respective resonance wavelengths are presented in Fig. 3(d). The enhancement factor in the metasurface of θ=1° is up to as large as 388. We next focus on the nonlinear response in the metasurface of θ=1°, which is feasible for the nanofabrication using state-of-art technology.

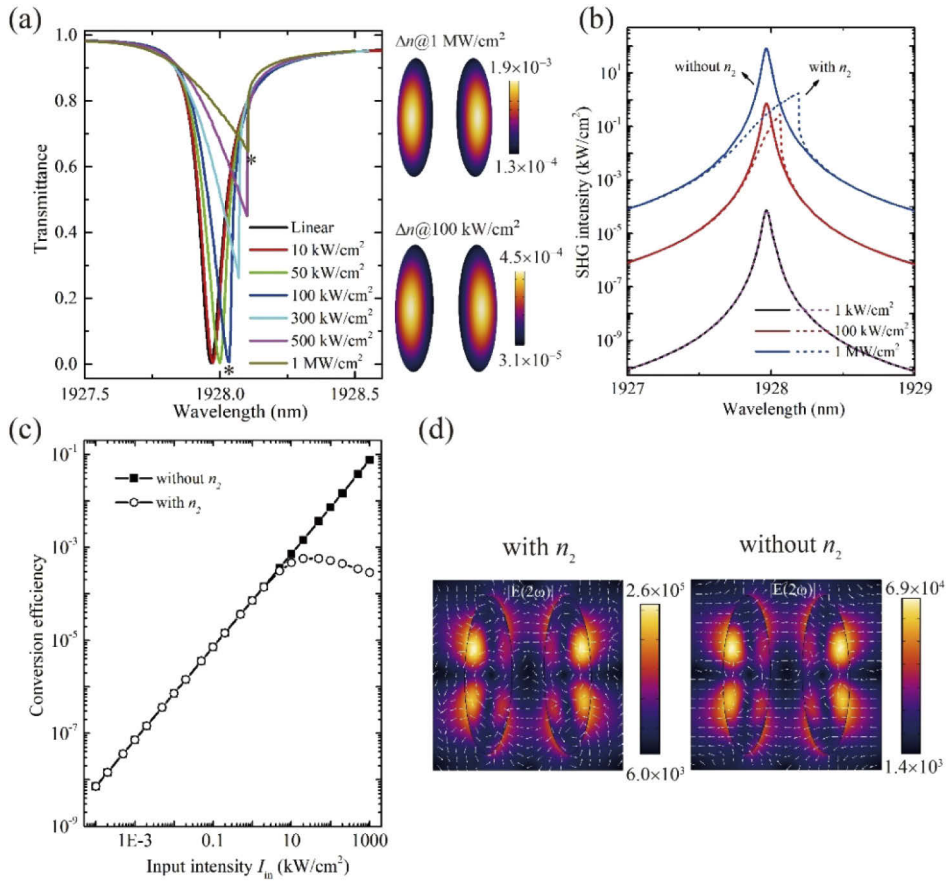

Fig. 4. (a) Linear transmission spectra under different pump intensities and the change of refractive index Δn of the AlGaAs bars at pump intensity of 100 kW/cm^2 and 1 MW/cm^2 at the resonance wavelength marked by star is shown, respectively. (b) SHG intensity spectra with and without considering the nonlinear refraction of AlGaAs under different pump intensities. (c) SHG conversion efficiency at the linear resonance wavelength, and (d) electric field distribution of |E(2ω)| at second harmonic frequency under the pump intensity 100 kW/cm^2, with and without considering the n_2 of AlGaAs in the metasurface of angle θ=1°.

Optics EXPRESS

The transmission of the asymmetric metasurface considering the nonlinear refraction of AlGaAs under different intensities of pump light was investigated, as shown in Fig. 4(a). The change of refractive index Δn of the AlGaAs bars at pump intensity of 100 kW/cm^2 and 1 MW/cm^2 at the respective resonance wavelength is also shown in Fig. 4(a). The maximum change of Δn around 4.5×10^{-4} and 1.9×10^{-3} at the two typical pump intensities are obtained, respectively. The similar behavior as in GMR nanostructure, the spectra also have a red-shift trend and the distorted line-shape with the increase of input intensity. Such changes then influence the SHG response in the metasurfaces, as shown in Fig. 4(b). Similar as in the GMR nanostructure, the SHG spectra are overlapped under the relatively low input intensity (e.g. 1 kW/cm^2) and derivate from each other when the change of refraction of AlGaAs dramatically affects the resonance condition (e.g. at the pump intensity of 100 kW/cm^2). If we also fix the concerning fundamental wavelength at the resonance wavelength of metasurface obtained from the linear transmission, the SHG conversion efficiency versus the input pump intensity is shown in Fig. 4(c). The maximum SHG conversion efficiency in the asymmetric nonlinear metasurface is around 5.7×10^{-4} at the pump intensity of 20 kW/cm^2, which is also much lower than the maximum conversion efficiency in the nanostructure of the value 7.6×10^{-2} without considering n_2 of AlGaAs at the pump intensity 1 MW/cm^2. The ultimate conversion efficiency in the asymmetric nonlinear metasurface considering the intrinsic n_2 of AlGaAs under the pump intensity 1 MW/cm^2 occurs at the wavelength around 1928.19 nm of the value 1.8×10^{-3}. The SHG field distributions $|E(2\omega)|$ with and without considering n_2 of AlGaAs under the pump intensity 100 kW/cm^2 are shown in Fig. 4(d). The distributions of SHG field are similar but values have large difference which explain the different conversion efficiency at the same pump intensity.

4. Conclusions

We investigated SHG response in all-dielectric GMR nanostructures and asymmetric metasurfaces working at quasi-BICs of high-Q factors with the consideration of intrinsic nonlinear refraction of dielectrics. The ultimate conversion efficiency in the nanostructures is obtained under the intense pump intensities. The results show that the expected SHG conversion efficiency in the nanostructures of high-Q factor under intense pump intensity is much lower than the traditionally calculated values without considering the nonlinear refraction of dielectrics. Since the third-order nonlinear refraction is an intrinsic property in all dielectrics, the conclusion is not limited in the AlGaAs-based resonators. Our investigation therefore has the significance for the design and understanding of efficient integrated nonlinear metasurfaces.

Funding. National Natural Science Foundation of China (91950104, 12074225, 91950106); Natural Science Foundation of Shandong Province (ZR2019MA024).

Disclosures. The authors declare no conflicts of interest.

Data availability. Data underlying the results presented in this paper are not publicly available at this time but may be obtained from the authors upon reasonable request.

References

1. M. Kauranen and A. V. Zayats, "Nonlinear plasmonics," Nat. Photonics **6**(11), 737–748 (2012).
2. K. Koshelev, S. Kruk, E. Melik-Gaykazyan, J.-H. Choi, A. Bogdanov, H.-G. Park, and Y. Kivshar, "Subwavelength dielectric resonators for nonlinear nanophotonics," Science **367**(6475), 288–292 (2020).
3. S. Keren-Zur, L. Michaeli, H. Suchowski, and T. Ellenbogen, "Shaping light with nonlinear metasurfaces," Adv. Opt. Photonics **10**(1), 309–353 (2018).
4. Z. Li, W. W. Liu, G. Z. Geng, Z. C. Li, J. J. Li, H. Cheng, S. Q. Chen, and J. G. Tian, "Multiplexed Nondiffracting Nonlinear Metasurfaces," Adv. Funct. Mater. **30**(23), 1910744 (2020).
5. W. Ye, F. Zeuner, X. Li, B. Reineke, S. He, C.-W. Qiu, J. Liu, Y. Wang, S. Zhang, and T. Zentgraf, "Spin and wavelength multiplexed nonlinear metasurface holography," Nat. Commun. **7**(1), 11930 (2016).
6. L. Huang, X. Chen, H. Mühlenbernd, H. Zhang, S. Chen, B. Bai, Q. Tan, G. Jin, K. W. Cheah, C.-W. Qiu, J. Li, T. Zentgraf, and S. Zhang, "Three-dimensional optical holography using a plasmonic metasurface," Nat. Commun. **4**(1), 2808 (2013).

Optics EXPRESS

7. C. Schlickriede, S. S. Kruk, L. Wang, B. Sain, and T. Zentgraf, "Nonlinear Imaging with All-Dielectric Metasurfaces," Nano Lett. **20**(6), 4370–4376 (2020).
8. X. Li, Y. Tan, L. Yin, Y. Huo, L. Zhao, Q. Yue, and T. Ning, "Bistability of optical harmonic generation in monolayer graphene plasmonics," Opt. Lett. **46**(5), 1029–1032 (2021).
9. M. W. Klein, C. Enkrich, M. Wegener, and S. Linden, "Second harmonic generation from magnetic metamaterials," Science **313**(5786), 502–504 (2006).
10. M. W. Klein, M. Wegener, N. Feth, and S. Linden, "Experiments on second- and third-harmonic generation from magnetic metamaterials," Opt. Express **15**(8), 5238–5247 (2007).
11. M. Celebrano, X. Wu, M. Baselli, S. Gromann, P. Biagioni, A. Locatelli, C. De Angelis, G. Cerullo, R. Osellame, B. Hecht, L. Duó, F. Ciccacci, and M. Finazzi, "Mode matching in multiresonant plasmonic nanoantennas for enhanced second harmonic generation," Nat. Nanotechnol. **10**(5), 412–417 (2015).
12. S. Liu, P. P. Vabishchevich, A. Vaskin, J. L. Reno, G. A. Keeler, M. B. Sinclair, I. Staude, and I. Brener, "An all-dielectric metasurface as a broadband optical frequency mixer," Nat. Commun. **9**(1), 2507 (2018).
13. Y. Kivshar, "All-dielectric meta-optics and non-linear nanophotonics," Natl. Sci. Rev. **5**(2), 144–158 (2018).
14. T. Ning, H. Pietatinen, O. Hyvärinen, R. Kumar, T. Kaplas, M. Kauranen, and G. Genty, "Efficient second-harmonic generation in silicon nitride resonant waveguide gratings," Opt. Lett. **37**(20), 4269–4271 (2012).
15. C. W. Hsu, B. Zhen, A. D. Stone, J. D. Joannopoulos, and M. Soljacic, "Bound states in the continuum," Nat. Rev. Mater. **1**(9), 16048 (2016).
16. S. T. Ha, Y. H. Fu, N. K. Emani, Z. Y. Pan, R. M. Bakker, R. Paniagua-Dominguez, and A. I. Kuznetsov, "Directional lasing in resonant semiconductor nanoantenna arrays," Nat. Nanotechnol. **13**(11), 1042–1047 (2018).
17. A. Kodigala, T. Lepetit, Q. Gu, B. Bahari, Y. Fainman, and B. Kante, "Lasing action from photonic bound states in continuum," Nature **541**(7636), 196–199 (2017).
18. Y. Chen, C. Zhao, Y. Z. Zhang, and C. W. Qiu, "Integrated Molar Chiral Sensing Based on High-Q Metasurface," Nano Lett. **20**(12), 8696–8703 (2020).
19. F. Yesilkoy, E. R. Arvelo, Y. Jahani, M. K. Liu, A. Tittl, V. Cevher, Y. Kivshar, and H. Altug, "Ultrasensitive hyperspectral imaging and biodetection enabled by dielectric metasurfaces," Nat. Photonics **13**(6), 390–396 (2019).
20. Z. H. Han and Y. J. Cai, "All-optical self-switching with ultralow incident laser intensity assisted by a bound state in the continuum," Opt. Lett. **46**(3), 524–527 (2021).
21. Z. Lin, Y. Xu, Y. Lin, J. Xiang, T. Feng, Q. Cao, J. Li, S. Lan, and J. Liu, "High-Q Quasi-bound States in the Continuum for Nonlinear Metasurfaces," Phys. Rev. Lett. **123**(25), 253901 (2019).
22. L. Carletti, K. Koshelev, C. De Angelis, and Y. Kivshar, "Giant Nonlinear Response at the Nanoscale Driven by Bound States in the Continuum," Phys. Rev. Lett. **121**(3), 033903 (2018).
23. L. Kang, H. Bao, and D. H. Werner, "Efficient second-harmonic generation in high Q-factor asymmetric lithium niobite metasurfaces," Opt. Lett. **46**(3), 633–636 (2021).
24. Z. Han, F. Ding, Y. Cai, and U. Levy, "Significantly enhanced second-harmonic generations with all-dielectric antenna array working in the quasi-bound states in the continuum and excited by linearly polarized plane waves," Nanophotonics **10**(3), 1189–1196 (2021).
25. D. Rocco, M. A. Vincenti, and C. De Angelis, "Boosting Second Harmonic Radiation from AlGaAs Nanoantennas with Epsilon-Near-Zero Materials," Appl. Sci. **8**(11), 2212 (2018).
26. D. Rocco, C. Gigli, L. Carletti, G. Marino, M. A. Vincenti, G. Leo, and C. De Angelis, "Vertical Second Harmonic Generation in Asymmetric Dielectric Nanoantennas," IEEE Photonics J. **12**(3), 1–7 (2020).
27. T. Ning, X. Li, Y. Zhao, L. Yin, Y. Huo, L. Zhao, and Q. Yue, "Giant enhancement of harmonic generation in all-dielectric resonant waveguide gratings of quasi-bound states in the continuum," Opt. Express **28**(23), 34024–34034 (2020).
28. F. Wu, J. Wu, Z. Guo, H. Jiang, Y. Sun, Y. Li, J. Ren, and H. Chen, "Giant Enhancement of the Goos-Hänchen Shift Assisted by Quasibound States in the Continuum," Phys. Rev. A **12**(1), 014028 (2019).
29. R. W. Boyd, *Nonlinear Optics* (Academic, 2003).
30. D. E. Aspnes, S. M. Kelso, R. A. Logan, and R. Bhat, "Optical properties of AlxGa1-xAs," J. Appl. Phys. **60**(2), 754–767 (1986).
31. R. W. Boyd, Z. Shi, and I. De Leon, "The third-order nonlinear optical susceptibility of gold," Opt. Commun. **326**, 74–79 (2014).
32. G. I. Stegeman, A. Villeneuve, J. Kang, J. S. Aitchison, C. N. Ironside, K. Al-hemyari, C. C. Yang, C.-H. Lin, H.-H. Lin, G. T. Kennedy, R. S. Grant, and W. Sibbett, "AlGaAs Below Half Bandgap: The Silicon of Nonlinear Optical Materials," J. Nonlinear Opt. Phys. Mater. **03**(03), 347–371 (1994).
33. M. Ohashi, T. Kondo, R. Ito, S. Fukatsu, Y. Shiraki, K. Kumata, and S. S. Kano, "Determination of quadratic nonlinear optical coefficient of AlxGa1-xAs system by the method of reflected second harmonics," J. Appl. Phys. **74**(1), 596–601 (1993).
34. S. Liu, M. B. Sinclair, S. Saravi, G. A. Keeler, Y. Yang, J. Reno, G. M. Peake, F. Setzpfandt, I. Staude, T. Pertsch, and I. Brener, "Resonantly enhanced second-harmonic generation using III–V semiconductor alldielectric metasurfaces," Nano Lett. **16**(9), 5426–5432 (2016).
35. K. Koshelev, S. Lepeshov, M. Liu, A. Bogdanov, and Y. Kivshar, "Asymmetric Metasurfaces with High- Q Resonances Governed by Bound States in the Continuum," Phys. Rev. Lett. **121**(19), 193903 (2018).